

Toward adaptive control of coherent electron transport in semiconductors

Fernando Solas, Jennifer M. Ashton, Andreas Markmann,^{a)} and Herschel A. Rabitz
Department of Chemistry, Princeton University, Princeton, New Jersey 08544, USA

(Received 19 August 2008; accepted 14 April 2009; published online 1 June 2009)

This work explores the feasibility of using shaped electrostatic potentials to achieve specified final scattering distributions of an electron wave packet in a two dimensional subsurface plane of a semiconductor. When electron transport takes place in the ballistic regime, and features of the scattering potentials are smaller than the wavelength of the incident electron then coherent quantum effects can arise. Simulations employing potential forms based on analogous optical principles demonstrate the ability to manipulate quantum interferences in two dimensions. Simulations are presented showing that suitably shaped electrostatic potentials may be used to separate an initially localized Gaussian wave packet into disjoint components or concomitantly to combine a highly dispersed packet into a compact form. The results also indicate that highly complex scattering objectives may be achieved by utilizing adaptive closed-loop optimal control in the laboratory to determine the potential forms needed to manipulate the scattering of an incoming wave packet. An adaptive feedback algorithm can be used to vary individual voltages of multipixel gates on the surface of a solid state structure to thereby find the potential features in the transport plane needed to produce a desired scattering objective. A proposed experimental design is described for testing the concept of adaptive control of coherent electron transport in semiconductors. © 2009 American Institute of Physics. [DOI: 10.1063/1.3132782]

I. INTRODUCTION

Continuing technological advances allowing for the fabrication of tailored heterostructures and external surface gates raise the possibility of creating subsurface potentials with special shapes. With these crafted potentials, subsurface electron wave packets may be scattered or recombined forming a type of complex quantum mechanical electron “switch yard”. Electrostatic potentials can act as lenses to redirect incoming ballistic electrons in analogy with the use of optical lenses.¹ The application of simple principles similar to those in optics provides a powerful means to identify the basic shape of potentials that can produce desired electron wave packet scattering patterns. The potentially complex outcome of quantum mechanical scattering with shaped potentials, however, indicates that introducing optimal design (control) techniques² will likely be necessary to achieve highly structured scattering objectives. Ultimately expressing the problem in an optimal control framework would allow for obtaining the best possible scattering outcomes which take into consideration practical constraints on generating the potentials.

The proposed concept of adaptive control of coherent electron transport in semiconductors (ACCENTS) involves the creation of an adaptive closed-loop device, whereby the subsurface potentials can be changed in an iterative fashion to determine their optimal shape as sketched in Fig. 1. Such a procedure would be similar to the broadly successful use of

adaptive control techniques to deduce the shape of ultrafast laser pulses for manipulating atomic and molecular quantum dynamics.²

In ACCENTS, an array of pixelated features with tunable time-independent surface voltages serve as the controls in analogy with the tunable pixels acting on frequency components in laser pulse shaping.^{3,4} One-dimensional electron reflection and transmission is highly sensitive to the shape of the static potentials,⁵ and optimal design techniques can identify potentials capable of producing the target reflection

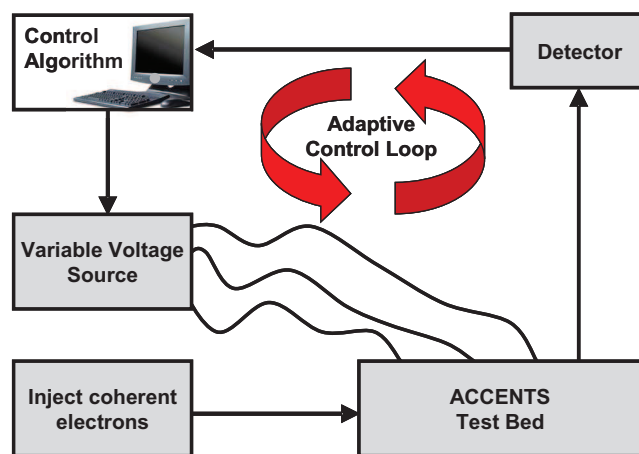


FIG. 1. (Color online) General configuration for ACCENTS including injection, detection, and adaptive closed-loop feedback control. The wires from the variable voltage source connect to individual pixelated surface gates with sufficient density and small size to create a desired scattering subsurface potential in the test bed material. A possible test bed design for the ACCENTS material is shown in Fig. 2.

^{a)}Electronic mail: markmann@princeton.edu.

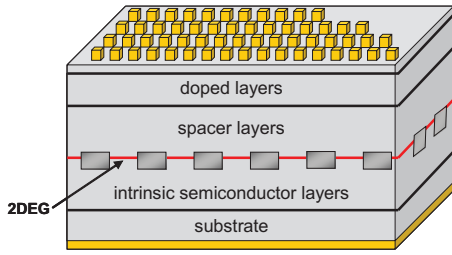


FIG. 2. (Color online) A possible configuration proposed as a test bed for ACCENTS: A variety of constructs exists to create an adjustable surface voltage array and for the subsurface materials. Here a high density array of metal surface dots is shown that may be individually connected via nanowires to a variable voltage regulator as shown in Fig. 1. The broken nature of the surface pixels is used to indicate that a wide variety of arrays is possible, including simpler arrangements at likely reduced spatial resolution.

and transmission coefficients;⁶ parallel behavior with electromagnetic scattering of optimized dielectric materials has been considered.⁷⁻⁹ It was proposed that one can direct the motion of a two-dimensional (2D) incoming electron wave packet via an optimally designed electrostatic spatial potential to produce a predetermined final state.⁶ The present work illustrates that complex scattering outcomes may be achieved in two dimensions using special potential shapes guided by optical principles, and also considers some of the physical parameters and operating conditions for achieving laboratory realization of a test bed for ACCENTS (Fig. 2).

A key desire is that the scattering take place in the ballistic regime, which leads to several constraints on the choice of material, physical device parameters, and operating conditions. Ballistic electron transport occurs in high-mobility semiconductors when the phase relaxation time is longer than the momentum relaxation time.^{10,11} An important feature of operating in the ballistic transport regime is the ability to maintain electron phase coherence. There are two main sources of electron phase decoherence. The first is electron-phonon interactions, which typically dominates at high temperatures. Below ~ 30 K, the most important phase decoherence mechanism in low dimensional systems is electron-electron collisions. Dephasing of 2D electrons in the ballistic regime was observed¹² at 1.4 K using a modulation-doped 2D electron gas (2DEG) formed in the interface between GaAs and $\text{Al}_x\text{Ga}_{1-x}\text{As}$. The results showed that a phase coherence length of ~ 10 μm was attained at an injection voltage of ± 1 meV. Operating at sufficiently low temperatures and low injection energies enables electron phase coherence for transport in the ballistic regime. In the 2DEG of high quality semiconductor heterostructures, ballistic transport can occur with a mean free path of up to several microns. Furthermore, the Fermi wavelength is large (30–80 nm) and can be comparable to the length of the electron transport channels. In the simplest case of ballistic transport in mesoscopic semiconductor structures, one may assume that electrons move from a source to a drain, through the active region without scattering, except from barriers inside the region or from the boundaries.¹⁰

A 2DEG with ballistic carriers may be present not only in interfaces but also in atomically thin materials such as graphene,^{13,14} which has been operated with tunable potential

barriers showing dominantly ballistic transport properties¹⁵ with theoretically predicted mean free paths of several hundred nanometers.¹⁶ Graphene is a particularly interesting material, since it exhibits suppression of backscattering.¹⁷

Ultrafast pump-probe Ti:sapphire femtosecond laser pulses have been used to both launch and detect ballistic electrons in devices fabricated utilizing the 2DEG formed in GaAs/AlGaAs heterostructures.¹⁸ The time-resolved transport in one such device at 4.2 K and under magnetic fields was measured with a resolution of less than 5 ps. In the present case, however, tunable electrostatic potentials rather than magnetic fields are used to steer the wave packet. The actual detailed layered design and materials of the ACCENTS test bed is open at this point.

The potential felt by the electrons in a plane below the surface of the semiconductor is determined by the electrostatic field described by Poisson's equation, and the potential depends on the dielectric constants of the materials forming the layers of the heterostructure, the distance between the charged surface pixels, and many other factors. In order to optimize the shape and strength of the overall electrostatic potential felt by the electrons in the 2DEG, a large array of small pixels with independently controlled voltages needs to be created. The construction of such an array is a nontrivial issue. The array components could be produced using one of many possible fabrication methods, e.g., layer-by-layer etching, chemical vapor deposition, nanowires (e.g., carbon nanotubes), nanodots, etc. Nanodots may be created and charged using scanning tunneling microscopy. Another possibility is to use charge coupled devices to provide a heterogeneous spatial charge pattern.¹⁹ For the laboratory realization of the test bed proposed in this paper, a method for the injection and detection of the electrons has to be selected.

Although there exists a number of possibilities for creating surface voltage arrays, some of these methods have extended three dimensional features, possibly restricting the subsurface potential shapes that may be constructed. For example, charged leads are extended and may distort the field from finely featured surface pixels. Thus, the choice of technology will play an important role in capability and flexibility for creating potential shapes. Ideally, the pixels would be on the nanometer scale but initial configurations could be more modest to illustrate the basic principles of ACCENTS. In practice, a key aspect of ACCENTS is its ability to operate optimally and possibly overcome construction exigencies as best as possible. The simulations presented in Sec. III assume there are no restrictions or limitations in regard to the shape of the potentials. A full simulation of ACCENTS is beyond the scope of this work, and simple potential shapes chosen *a priori* will be used guided by analogous optical principles.

This paper aims to illustrate the scattering capabilities of an ACCENTS device. In Sec. II, a quantum mechanical model is presented to describe the ballistic transport, scattering and phase coherence of an electron wave packet in the 2DEG at the interface of a semiconductor heterostructure. Section III presents scattering simulations with single poten-

tial barriers with concave and convex features. Section IV summarizes the findings and outlines additional future work on ACCENTS.

II. SCATTERING MODEL

Electrons in a 2DEG may be subjected to a potential $V_0(x,y)$, resulting from donor ions or impurities and defects in the doped layers of the heterostructure. A separate potential $V'(x,y)$, arises from the surface voltage pixel array. Thus, the total potential felt by an electron in the 2DEG is the sum $V=V_0+V'$. In future work, adaptive control techniques will be applied to optimize V' , allowing for more complex scattering outcomes than the simple simulations presented in Sec. III. The shape of V' may be restricted by practical considerations, hence limiting the available potential forms. However, in the present work, no restrictions are placed on V' so that V can also take any shape, if necessary by cancellation of by counter terms in V_0 . Operation of ACCENTS under closed loop will seek the best form for V' to meet the posed objectives, possibly in cooperation with V_0 in some cases. Therefore, the following simulations consider only the arbitrary total potential V . The Hamiltonian for the system is time independent with the form: $H=(p_x^2+p_y^2/2m)+V(x,y)$.

High mobility 2DEGs in semiconductor heterostructures (e.g., GaAs/Al_xGa_{1-x}As) have attractive properties.²⁰ In practice, many complicating physical effects can be operative beyond those contained in the Hamiltonian above. As an initial study, a simple description is adopted here in which all the material effects are subsumed into the effective mass approximation. Thus, consider an electron of effective mass m described by the wave packet $\psi(x,y,t)$ satisfying the time dependent Schrödinger equation,

$$i\hbar \frac{\partial \psi(x,y,t)}{\partial t} = \left[-\frac{\hbar^2}{2m} \left(\frac{\partial^2}{\partial x^2} + \frac{\partial^2}{\partial y^2} \right) + V(x,y) \right] \psi(x,y,t), \quad (1)$$

with a specified initial condition $\psi(x,y,0)=\phi(x,y)$. In Sec. III, the effective mass is $m=0.067m_e$ corresponding to the GaAs material.

The scattering occurs in the xy -plane with total dimensions on the order of $5.0 \mu\text{m}$ in each direction. A grid of 512×512 points was used to represent the potential and the wave function. All of the illustrations in Sec. III result from using an initial wave packet of Gaussian form,

$$\phi(x,y) = \exp(ik_x x) \exp \left[-\frac{(x-x_0)^2}{2\sigma_x^2} - \frac{(y-y_0)^2}{2\sigma_y^2} \right]. \quad (2)$$

The initial wave packet has the width $\sigma_x=\sigma_y=150 \text{ nm}$ and the wave vectors, $k_x=72.6 \times 10^{-6} \text{ m}^{-1}$ and $k_y=0$, corresponding to motion in the positive x -direction. The wave packet has an associated energy of 3.104 meV , with a de Broglie wavelength of 86 nm , and the features of the scattering potential are on the same length scale. In all of the simulations the time step was 0.025 fs and the Schrödinger equation was numerically integrated using a Chebyshev propagator,²¹ which is an efficient long time propagator for time-independent Hamiltonian operators allowing the calcu-

lations to be performed in tens of minutes on commodity computer hardware.

The packet evolved for a sufficiently long time to carry it beyond the region where the potential $V(x,y)$ had any significant magnitude. In all of the cases considered here, the potential is locally repulsive, $V(x,y) \geq 0$, centered at one or more specified locations in the overall scattering plane. Each of the potentials was of constant flat value within a domain boundary of shape $\Omega(x,y)$ with a smooth Gaussian fall off of the form $\exp[-d^2(x,y)/2\sigma^2]$ outside of the boundary. Here $d(x,y)$ is the local distance normal to $\Omega(x,y)$ and $\sigma=34 \text{ nm}$, corresponding to a feature width which is within current photolithographic technology, although a reduction in resolution will likely occur in the subsurface transport plane. The barrier height was chosen to be less than the electron kinetic energy to permit a reasonable level of transmission and directional control over the scattering.

III. ILLUSTRATIONS

This section presents several simulations illustrating the nature of scattering outcomes that may be achieved using 2D potentials with local concave or convex features. The illustrations shown were chosen to especially point out that significant control over scattering may be achieved by even simple potential forms. Each figure shows the potential, the initial packet at $t=0$ and the final packet at a later fixed time T .

A. Dispersive scattering

1. Single potential

The potential in this case is the rhomboid-type structure shown at the center of Fig. 3, with two distinct concave features on its transmissive side and a barrier height of 2.78 meV . Note that interpretation of potential features as being concave or convex is largely a matter of definition in relation to a chosen reference potential shape. Approximately 50% of the packet is transmitted to the right and the remainder is reflected. The main features of the scattering pattern shown at the final time of $T=27 \text{ ps}$ have an accumulated probability density of 96%, with the remaining 4% spread rather evenly over the rest of the scattering domain. The concavity of the two aft lens features in the potential are important for creating the pair of transmitted, symmetrically located, focused packets to the right of the scattering potential. The principle of utilizing concave lens structures was found to be generally operative for this purpose in a variety of simulations. If the aft surfaces are flat or convex in the same locations, then the transmitted scattering features are not as well focused.

2. Double scattering barriers

In this case, two potentials are included of the same general form as in Fig. 3 with their locations indicated in Fig. 4. The second potential was placed to lie in the path of one of the primary transmitted scattering features emanating from the potential of Fig. 3 and rising into the upper right portion of that figure. The latter portion of the wave packet was rescattered by the second potential, producing four pieces,

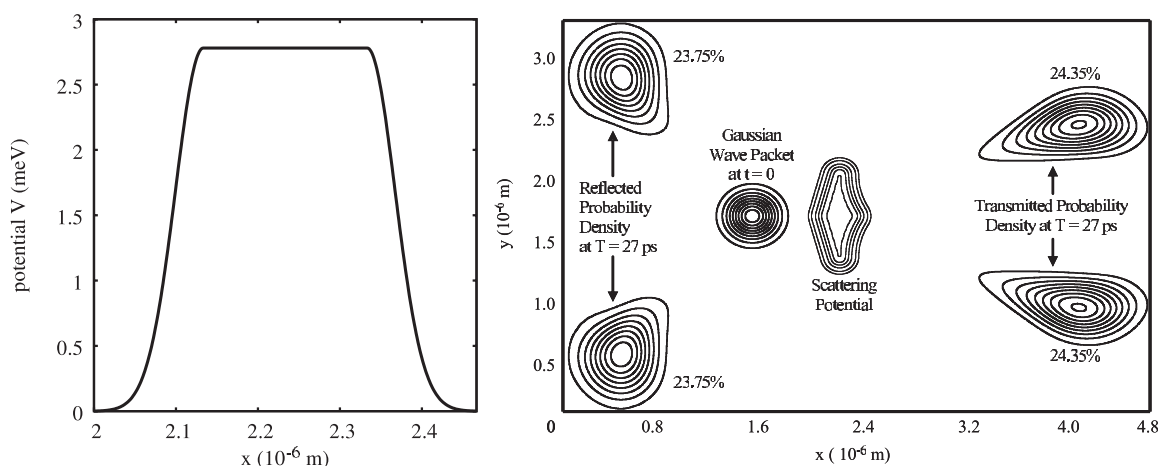


FIG. 3. Scattering with a single rhomboid shaped potential structure having two concave aft faceted features. The potential is flat with Gaussian falloff of length scale $\sigma=34$ nm. The left panel shows a cross section along the line $y=0$ to illustrate this. In the right panel, as well as the following figures, the square modulus of the wave function $|\psi(x,y,t)|^2$ and the potential $V(x,y)$ are shown as contour lines. The final wave packet is at $T=27$ ps. The percentages refer to the probability density contributions from the localized packet features; the same labeling is used in Figs. 4–6.

one of which contained 36% of the final probability density as shown in the lower right corner of Fig. 4. This latter complex packet is a superposition of a primary piece coming from the initial scattering potential and a secondary piece from the second potential structure, clearly illustrating quantum interference effects. Both potential barriers have a height of 2.61 meV, but the second barrier has an elongated aft component, and is rotated. This modifies the wave packet components transmitted through the second rhomboid so that their intersection with those from the first leads to the interferences seen in the lower right side of Fig. 3. Adjustment of the potential features can readily redirect the scattering flux pattern. Only a few alterations of the potential were required to tune the scattering patterns in a desired fashion; this behavior suggests that the closed-loop iterative operations in Fig. 1 may be quite efficient and effective.

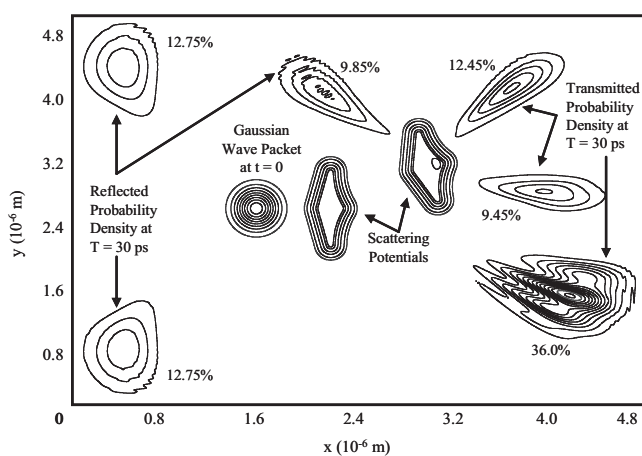


FIG. 4. Scattering of an incoming Gaussian wave packet by two rhomboid shaped potentials into multiple wave packet components with indicated probability density contributions at the final time $T=30$ ps. The small dark oval inside the second scattering barrier corresponds to a tiny portion of the wave function still located inside the potential at the final time T . The harmonic noise visible in the final wave packets is an artifact of the contour line drawing algorithm.

3. Single complex scattering potential

The single four-sided rhomboid potential in Fig. 3 produced four distinct scattering features. Introducing a second rhomboid potential in Fig. 4 resulted in additional features including one piece of the wave packet that arose from a coherent superposition between the scattering from both potentials. This principle is explored further in Fig. 5 with a more complex single scattering potential having eight faceted lens features on its surface and a potential height of 2.61 meV. All of these potential facets are on the same length scale as the packet wavelength, on the order of 85–105 nm. Figure 5 shows the scattering pattern achieved after propagation for $T=30$ ps. The initial packet is split into eight distinct dominant features all having approximately equal probabilities ranging from 9.6% to 14.4%. A smaller back reflected peak is also evident containing $\sim 1\%$ of the probability. Considering the rich scattering pattern produced in this example and the ability to rescatter against multiple po-

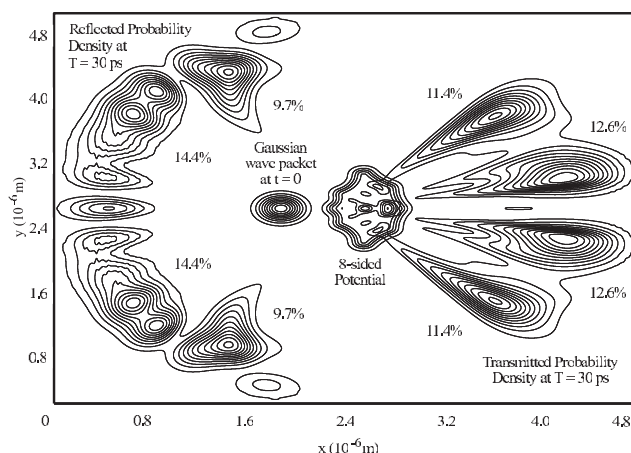


FIG. 5. Scattering from an octagonal faceted potential having concave features resulting in eight primary components of the final wave packet with probability distribution percentages ranging from 9.6% to 14.4% as indicated at time $T=30$ ps. The structure superimposed on the potential is part of the final wave function at time T .

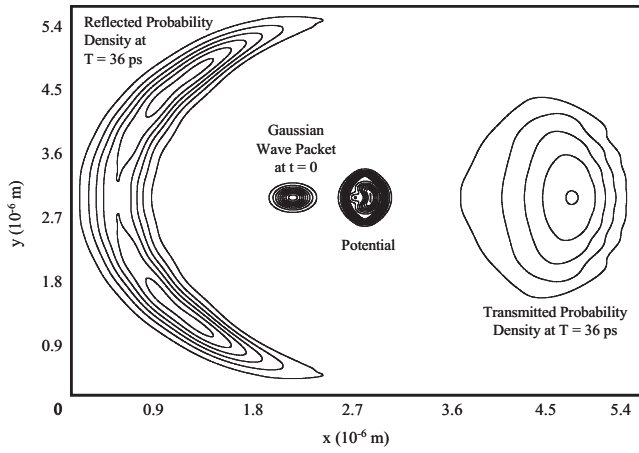


FIG. 6. Scattering from a featureless distorted circular potential into single final transmitted and reflected components at time $T=36$ ps. The structure inside the potential represents pieces of the wave packet that have not yet escaped.

tentials, as shown in Fig. 4, it is evident that various combinations of scattering potentials with simple features can create highly complex states from a simple Gaussian initial wave packet.

4. Featureless potentials

In all the cases above, only simple scattering principles analogous to those in optics were employed to intuitively determine potential shapes that can result in rich scattering structures. These principles rested on creating potential lens structures of a size on the order of the wavelength of the incident electron (~ 86 nm). The final example points out the significance of the latter principle by taking the limit of having a potential that is of a featureless lens shape but still of constant barrier height 2.875 meV. The potential is the slightly flattened circle shown in Fig. 6 where only single transmitted and reflected packets are evident. Starting with the eight-sided potential in Fig. 5, and increasing the number of facets while decreasing their size, will inevitably lead to a loss of control over the final scattering structure, as illustrated in Fig. 6. In between these limits, any variety of cases can be envisioned including, for example, adding a single faceted lens to the otherwise smooth potential in Fig. 6 to create a single additional scattering feature as desired, etc.

B. Spatially reconstitutive scattering

In each illustration in Sec. III A, a well-defined narrow incoming Gaussian wave packet was dispersed into a number of subcomponents, which were directed across the planar scattering region. The incident packet might have been generated by an ultrafast laser pulse to place it in the scattering domain with the appropriate kinetic energy. Other circumstances may be envisioned, where the initial wave packet itself has a highly complex form with various spatially dispersed components moving in distinct directions. Such initial wave packets might be formed by spatial-temporal shaped laser pulses or possibly from the scattering of multiple potentials as in Fig. 4. The present illustration suggests that it is, in principle, possible to create a suitable potential shape

that may act to recombine a number of incoming packet portions into a single localized structure. The construction of such reconstitutive potentials nominally would require the introduction of optimal design adaptive feedback techniques inherent in ACCENTS due to the complexity of the task involved, which calls for taking into account the detailed nature of the initial dispersed packet. However, even without optimization, consideration of the dispersive scattering achieved with the octagonal potential in Fig. 5 may be re-analyzed to illustrate that this is possible, in principle.

Treating the final wave packet as the starting condition for Eq. (1) and marching backward in time from $t=T$ to $t=0$ will lead to a reconstitution of the initial packet shown in Fig. 6. Although this process is mathematically correct, in the laboratory one cannot run the clock backward in time. However, consider an initial wave packet $\tilde{\phi}(x, y)$ of the form

$$\tilde{\phi}(x, y) = \psi^*(x, y, T) = \text{Re } \psi(x, y, T) - i \text{Im } \psi(x, y, T). \quad (3)$$

The assumption here is that the packet was created by some means such as a suitable spatiotemporal laser pulse with the net result being the complex conjugate of the scattering wave function at time $t=T$ in Fig. 5. To illustrate the dynamics moving forward in time from $t=0$ to time $t=T$ under the initial condition it is convenient to rewrite Eq. (1) in terms of its real and imaginary parts:

$$\begin{aligned} \hbar \frac{\partial \text{Re } \psi(x, y, t)}{\partial t} &= \left[-\frac{\hbar^2}{2m} \left(\frac{\partial^2}{\partial x^2} + \frac{\partial^2}{\partial y^2} \right) + V(x, y) \right] \\ &\quad \times \text{Im } \psi(x, y, t), \\ -\hbar \frac{\partial \text{Im } \psi(x, y, t)}{\partial t} &= \left[-\frac{\hbar^2}{2m} \left(\frac{\partial^2}{\partial x^2} + \frac{\partial^2}{\partial y^2} \right) + V(x, y) \right] \\ &\quad \times \text{Re } \psi(x, y, t). \end{aligned} \quad (4)$$

Now consider working with the complex conjugate wave function $\tilde{\psi} = \text{Re } \psi - i \text{Im } \psi$. The tilde is used to denote that the complex conjugate wave function is being used where the initial condition is $\tilde{\psi}(x, y, 0) = \tilde{\phi}(x, y) = \psi^*(x, y, T)$. It is easy to show from Eq. (4) that $\tilde{\psi}$ satisfies

$$\begin{aligned} \hbar \frac{\partial \text{Re } \tilde{\psi}(x, y, \tau)}{\partial \tau} &= \left[-\frac{\hbar^2}{2m} \left(\frac{\partial^2}{\partial x^2} + \frac{\partial^2}{\partial y^2} \right) + V(x, y) \right] \\ &\quad \times \text{Im } \tilde{\psi}(x, y, \tau), \\ -\hbar \frac{\partial \text{Im } \tilde{\psi}(x, y, \tau)}{\partial \tau} &= \left[-\frac{\hbar^2}{2m} \left(\frac{\partial^2}{\partial x^2} + \frac{\partial^2}{\partial y^2} \right) + V(x, y) \right] \\ &\quad \times \text{Re } \tilde{\psi}(x, y, \tau), \end{aligned} \quad (5)$$

where $\tau = -t$. Consider time-reversal of the process in Fig. 5, starting from a state with four components on the right and several on the left (τ) and ending in a single wave packet after (time-reversed) scattering at the potential. Taking the potential away results in the wave function components intersecting each other without interaction and diverging from each other at later times. It is the insertion of the potential that combines these components into one spatially localized wave

packet that retains its integrity for long times (as it results as a localized Gaussian wave packet with a momentum in the negative x -direction, evolving away from the scattering potential). Simulation of this process was performed using complex conjugate final states from the previous simulations as initial states and integrating forward in time. The result demonstrates that, in spite of the complexity, these processes are available for systematic study using closed-loop optimization.

IV. DISCUSSION

In the illustrations presented in Sec. III, simple techniques guided by analogous principles from optics were employed to assess what might be achieved by applying optimal design procedures and ultimately closed-loop adaptive control directly in the laboratory as indicated in Fig. 1, thereby demonstrating the basic configuration of ACCENTS. High degrees of focusing and steering of a wave packet can be achieved by simple concave or convex local lens structures forming the bounding surface $\Omega(x, y)$ of the scattering potential domain. The simulations indicate that highly structured scattering patterns may be created, provided that the potential lens features are of a size comparable to the wavelength of the incident electron.

In the proposed work on ACCENTS, the detailed shape of the potential $V(x, y)$ in Eq. (1) would be subjected to optimal design (i.e., through laboratory feedback) techniques such that the wave function $\psi(x, y, t)$ or its associated output current $\vec{j}(x, y, T) = \frac{\hbar}{m} \text{Im}[\psi^* \vec{\nabla} \psi]$ either have specified spatial forms at a target time T or integrated over time. There are two possibilities for measuring the scattering outcome of each potential configuration. The first is to determine the amount of charge that has arrived at a given point in space, up to time T , by integrating over the current $\int_0^T \vec{j} \cdot \vec{n} dt$, where \vec{n} is a unit vector pointing along the direction of current collection. The second possibility is to control the temporal form of the current, calling for time-resolved measurements, which are more challenging experimentally. In either case, the simulations presented herein suggest that the application of adaptive closed-loop optimal control to ballistic electron transport in solid state systems appears promising as a means to maintain electron phase coherence and to meet complex target wave packet distributions. The test bed for ACCENTS proposed in this work can be constructed in a hierarchical fashion starting with even a few simple surface gate forms before ultimately moving toward a full high density array.

This paper illustrates the rich nature of manipulating 2D quantum mechanical electron scattering dynamics in semiconductor heterostructures by means of the introduction of custom tailored electrostatic potentials. The potentials can be used to filter and/or modify both the phases and amplitudes of the Fourier (or other convenient representation) components of an incoming wave packet. Figure 5 shows that multiple scattering potentials can be positioned in such a way as to harness the power of quantum mechanical interference and use it to create final wave packets of desired composition. Reversing the process in Fig. 5 demonstrates that even

highly complex initial wave packets may be controlled in their scattering by properly shaped potentials. The ability to use simple intuitive principles from optics to identify effective potential shapes is very encouraging. The next step is to express this process in an optimal control framework in order to obtain the best possible potentials including any constraints on their forms and faceted features and to achieve complex scattering outcomes for which the potentials cannot be determined by intuition alone. In the laboratory, a realization of this concept would arise from the creation of adaptive closed-loop devices as discussed in Sec. I and schematically illustrated in Fig. 1. Such a procedure is analogous to the broadly successful use of adaptive control techniques to deduce the shape of ultrafast laser pulses for manipulating atomic and quantum molecular dynamics.² However, this proposal is distinct from traditional quantum control in that the controls are spatially dependent electrostatic potentials instead of time varying electric fields. Importantly, operation of ACCENTS takes into account the full control capabilities of the constructed device as well as an inherent potential structure V_0 in the solid state material. The adaptive closed-loop procedure will learn the best operations to either fight against or cooperate with this structure, as needed in order to reach the target objectives.

ACKNOWLEDGMENTS

The authors acknowledge support from the NSF and the Humboldt Foundation.

- ¹U. Sivan, M. Heiblum, C. Umbach, and H. Shtrikman, *Phys. Rev. B* **41**, 7937 (1990).
- ²R. Judson and H. Rabitz, *Phys. Rev. Lett.* **68**, 1500 (1992).
- ³H. Rabitz, *Science* **299**, 525 (2003).
- ⁴H. Rabitz, *Science* **314**, 264 (2006).
- ⁵X. Ying, M. Shayegan, S. Lyon, M. Littman, P. Gross, and H. Rabitz, *Appl. Phys. Lett.* **65**, 1154 (1994).
- ⁶P. Gross, H. Rabitz, M. Littman, S. Lyon, and M. Shayegan, *Phys. Rev. B* **49**, 11100 (1994).
- ⁷D. Pant, R. Coalson, M. Hernandez, and J. Campos-Martinez, *J. Light-wave Technol.* **16**, 292 (1998).
- ⁸D. K. Pant, R. D. Coalson, M. I. Hernández, and J. Campos-Martínez, *Appl. Opt.* **38**, 3917 (1999).
- ⁹P. Seliger, M. Mahvash, C. Wang, and A. Levi, *J. Appl. Phys.* **100**, 034310 (2006).
- ¹⁰S. Datta, *Electronic Transport in Mesoscopic Systems* (Cambridge University Press, Cambridge, 1995).
- ¹¹S. Datta, *Quantum Transport: Atom to Transistor* (Cambridge University Press, Cambridge, 2005).
- ¹²A. Yacoby, *Phys. Rev. Lett.* **66**, 1938 (1991).
- ¹³K. Novoselov, A. Geim, S. Morozov, D. Jiang, Y. Zhang, S. Dubonos, I. Grigorieva, and A. Firsov, *Science* **306**, 666 (2004).
- ¹⁴A. Geim and K. Novoselov, *Nature Mater.* **6**, 183 (2007).
- ¹⁵B. Huard, J. Sulpizio, N. Stander, K. Todd, B. Yang, and D. Goldhaber-Gordon, *Phys. Rev. Lett.* **98**, 236803 (2007).
- ¹⁶C. Berger, Z. Song, T. Li, X. Li, A. Y. Ogbazghi, R. Fend, Z. Dai, A. N. Merchenkov, E. H. Conrad, P. N. First, and W. A. de Heer, *J. Phys. Chem. B* **108**, 19912 (2004).
- ¹⁷T. Ando, T. Nakanishi, and R. Saito, *J. Phys. Soc. Jpn.* **67**, 2857 (1998).
- ¹⁸E. Shaner and S. Lyon, *Phys. Rev. Lett.* **93**, 037402 (2004).
- ¹⁹K. Mutamba, A. Sigurdardottir, and H. Hartnagel, *Analog Integr. Circuits Signal Process.* **24**, 37 (2000).
- ²⁰H. Haug and S. Koch, *Quantum Theory of the Optical and Electronic Properties of Semiconductors* (World Scientific, Singapore, 2004).
- ²¹C. Leforestier, R. Bisseling, C. Cerjan, M. Feit, R. Friesner, A. Gulberg, and R. Koslo, *J. Comput. Phys.* **94**, 59 (1991).